Crystal Structure and Thermal Behaviour of $Er_2(SeO_4)_3 \cdot 8H_2O$

Ina Krügermann and Mathias S. Wickleder

Institut für Anorganische Chemie, Universität zu Köln, Greinstraße 6, D-50939 Köln, Germany

Reprint requests to PD Dr. Mathias S. Wickleder. Fax: +49 (0)221 470 5083.
E-mail: m.wickleder@uni-koeln.de

Z. Naturforsch. **59b,** 958 – 962 (2004); received June 8, 2004

Dedicated to Professor Kurt O. Klepp on the occasion of his 60th birthday

Single crystals of $Er_2(SeO_4)_3 \cdot 8H_2O$ were obtained by dissolving Er_2O_3 in selenic acid. The selenate crystallizes in the monoclinic space group $C2/c$ ($Z = 4$, $a = 1372.8(2)$, $b = 687.51(7)$, $c = 1860.2(3)$ pm, $\beta = 101.85(2)^\circ$, $R_{all} = 0.0518$) and contains the Er^{3+} ions in eightfold coordination of oxygen atoms that belong to two crystallographically different SeO_4^{2-} ions and to four H_2O molecules. According to DTA/TG measurements and temperature dependent powder diffraction data, $Er_2(SeO_4)_3 \cdot 8H_2O$ decomposes in several steps yielding finally Er_2O_3. $Er_2(SeO_4)_3$ and $Er_2(SeO_3)_3$ could be identified as intermediates, and for $Er_2(SeO_4)_3$ a phase transition was detected.

Key words: Erbium, Selenate, Selenite, Crystal Structure, Thermal Analysis

Introduction

Selenates of the rare earth elements have been investigated to a much lesser extent than the respective sulfates. Based on our present knowledge their structural chemistry parallels essentially the one of the respective sulfates as might be expected from the analogous structure and the comparable volume of the selenate and sulfate anion [1]. On the other hand, the thermal behaviour of sulfates and selenates is usually remarkably different. Lanthanide sulfates decompose at temperatures above 900 °C leading to oxide-sulfates and finally to oxides [2]. The decomposition of selenates starts at lower temperatures and leads in a first step to the respective rare earth selenites [3]. This is due to higher stability of Se(IV) compared to S(IV). We used this decomposition reaction to prepare single crystals of lanthanide selenites for the first time some years ago [4]. At high temperature the selenites decompose to oxides, probably with the oxide-selenites $M_2(SeO_3)O_2$ as intermediates. The latter have not yet been characterized structurally, but their existence has been proved by thermochemical investigations [5]. Other intermediates might be the oxide-selenites $M_2(SeO_3)_2O$, for which the structure of the terbium compound is known [6]. Selenates of the rare earth elements are most conveniently obtained from the reaction of the respective sesquioxides with selenic acid. They crystallize as hydrates, most often with eight molecules of crystal water [1]. In this paper we describe the preparation and crystal structure of $Er_2(SeO_4)_3 8H_2O$ and its complete decomposition followed by means of DTA/TG measurements and temperature dependent powder diffraction.

Experimental Section

Pink single crystals of $Er_2(SeO_4)_3 \cdot 8H_2O$ were grown by evaporation of a solution that had been obtained by dissolving Er_2O_3 in selenic acid (20% H_2SeO_4). Selenic acid has previously been prepared from H_2O_2 and SeO_2 according to the procedure given in [7]. Some of the prism-shaped crystals were mounted in glass capillaries and their quality was checked by means of orientation images on a single crystal diffractometer (STOE IPDS I). For the best specimen reflection intensity data were collected using the same diffractometer. With respect to the lattice parameters, $Er_2(SeO_4)_3 \cdot 8H_2O$ is isotypic with the respective sulfate. Assuming the space group ($C2/c$) and the positional parameters of the latter, a reliable structure model was refined using the program SHELXL93 [8]. The data were corrected numerically for absorption effects [9]. Details of the measurement and the crystallographic data are given in Tables 1 – 3 and are additionally available from the Fachinformationszentrum Karlsruhe, D-76344 Eggenstein-Leopoldshafen (crysdata@FIZ-Karlsruhe.de) on quoting the deposition number given in Table 1.

DTA/TG measurements were performed with the help of a thermal analyzer (STA 409, NETZSCH). For that pur-

Table 1. Crystallographic data of $Er_2(SeO_4)_3 \cdot 8H_2O$.

Lattice parameters	$a = 1372.8(2)$ pm
	$b = 687.51(7)$ pm
	$c = 1860.2(3)$ pm
	$\beta = 101.85(2)^\circ$
Cell volume	1718.2(4) Å^3
No. of formula units	4
Crystal system	monoclinic
Space group	$C2/c$ (No. 15)
Diffractometer	Stoe IPDS-I
Radiation	Mo-K$_\alpha$ (graphite-monochrom., $\lambda = 71.07$ pm)
Temperature	20 °C
Data range	$5^\circ < 2\theta < 52^\circ$
Index range	$-16 \le h \le 16$
	$-8 \le k \le 8$
	$-22 \le l \le 22$
Rotation angle; φ-increment	$0^\circ < \varphi < 200^\circ$; 2.0°
No. of images	100
Exposure time	5 min
Detector distance	60 mm
Data corrections	polarization/Lorentz
Absorption correction	numerical [9]
μ	161.2 cm^{-1}
No. of collected reflections	6580
No. of unique reflections	1693
No. of reflections with $I_o > 2\sigma(I)$	1246
R_{int}	0.0813
Structure refinement	SHELXL-93 [8]
Scattering factors	Intern. Tables, Vol. C [15]
Goodness of fit	0.823
$R1$; $wR2(I_o > 2\sigma(I_o))$	0.0276; 0.0554
$R1$; $wR2$ (all data)	0.0518; 0.0570
CSD	414182

Table 2. Atomic positions and equivalent isotropic displacement parameters for $Er_2(SeO_4)_3 \cdot 8H_2O$.

Atom	Wyckoff site	x	y	z	U_{eq} $\cdot 10^{-1}$ [pm^2]
Er1	8f	0.66356(4)	0.01880(8)	0.39345(3)	5.4(1)
Se1	8f	0.78155(7)	0.5265(2)	0.40879(5)	4.8(2)
Se2	4e	1/2	0.3279(2)	1/4	5.6(3)
O11	8f	0.8396(5)	0.538(1)	0.3410(3)	12(2)
O12	8f	0.7409(6)	0.309(1)	0.4195(4)	15(2)
O13	8f	0.6896(5)	0.680(1)	0.3974(4)	7(2)
O14	8f	0.6400(5)	0.917(1)	0.5132(4)	9(2)
O21	8f	0.5917(6)	0.192(1)	0.2894(4)	16(2)
O22	8f	0.4620(5)	0.460(1)	0.3126(4)	13(2)
O1	8f	0.7551(5)	0.984(1)	0.3038(3)	15(2)
O2	8f	0.6642(5)	0.524(1)	0.5412(4)	11(2)
O3	8f	0.5428(5)	0.234(1)	0.4366(4)	12(2)
O4	8f	0.0156(6)	0.345(1)	0.3593(4)	17(2)

$U_{eq} = 1/3[U_{22} + 1/\sin^2\beta(U_{11} + U_{33} + 2U_{13}\cos\beta)]$ [16].

pose about 15 mg of the substance was filled in a corundum container and heated with a constant rate of 10 K/min under flowing argon. The thermal decomposition was followed from 300 up to 1220 K. For the DTA data a baseline correction was applied. Characteristic points like onset and end temperatures of the thermal effects were taken from the differentiated DTA curve following common procedures using the software delivered with the analyzer [10].

Table 3. Selected distances (pm) and angles (deg) for $Er_2(SeO_4)_3 \cdot 8H_2O$.

Er-O12	226.5(7)	Se1-O12		162.2(7)
-O1	229.8(6)	-O13		162.7(7)
-O21	231.3(7)	-O11		162.6(6)
-O4	233.0(8)	-O14		166.6(7)
-O13	235.3(7)			
-O14	241.8(7)	Se2-O21	(2x)	161.9(7)
-O2	244.3(6)	-O22	(2x)	164.3(7)
-O3	247.5(7)			
O12-Se1-O13	109.7(4)	O21-Se2-O21		109.3(6)
O12-Se1-O11	111.9(4)	O22-Se2-O22		113.1(6)
O13-Se1-O11	111.0(4)	O21-Se2-O22	(2x)	108.0(4)
O12-Se1-O14	106.5(4)	O22-Se2-O21	(2x)	109.2(4)
O13-Se1-O14	108.0(4)			
O11-Se1-O14	109.5(4)			

Temperature dependent powder diffraction data were collected using a powder diffractometer (Stadi P, STOE&CIE) equipped with a position sensitive detector and a graphite furnace providing a temperature accuracy of ±0.3 °C. The finely powdered sample was filled in a silica capillary ($\oslash$ = 0.3 mm) and sealed with grease. Data were collected in Debye-Scherrer geometry in the range of $2\theta = 7^\circ - 60^\circ$. The temperature range was 50 to 900 °C with intervals of 25 °C between 50 and 200 °C, and 50 °C between 200 and 900 °C. After each heating period the system was allowed to equilibrate for 30 min. The data were processed applying smoothing and background corrections using the program package VISUAL X^{POW} (STOE&CIE) [11]. The same program also allowed for lattice parameter refinements based on least square procedures.

Results and Discussion

Crystal structure

$Er_2(SeO_4)_3 \cdot 8H_2O$ (monoclinic, $C2/c$, $Z = 4$, $a = 1372.8(2)$, $b = 687.5(1)$, $c = 1860.2(3)$ pm, $\beta = 101.85(2)^\circ$) is isotypic with the respective erbium sulfate hydrate [12]. In accordance with the smaller volume of SO_4^{2-} compared to SeO_4^{2-} the lattice parameters of $Er_2(SO_4)_3 \cdot 8H_2O$ ($a = 1346.4(3)$, $b = 667.2(1)$, $c = 1816.1(6)$ pm, $\beta = 101.90(3)^\circ$) are remarkably smaller. In the crystal structure of $Er_2(SeO_4)_3 \cdot 8H_2O$ the Er^{3+} ions are in eightfold coordination of oxygen atoms that belong to four water molecules and four monodentate selenate groups. The distances Er-O range from 226.5(7) up to 247.5(7) pm (Table 3) and compare well with the data for the respective sulfate. One of the two crystallographically different se-

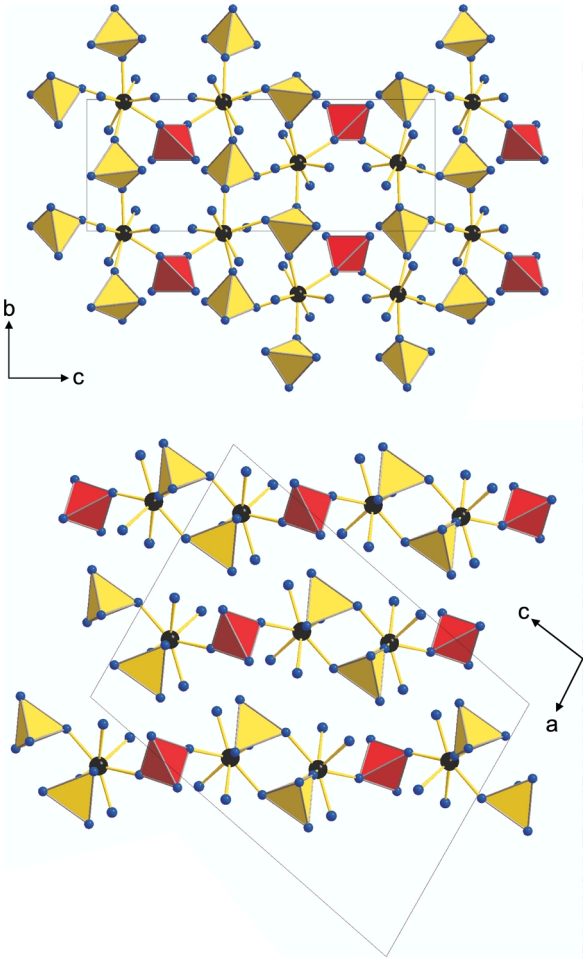

Fig. 1. Crystal structure of $Er_2(SeO_4)_3 \cdot 8H_2O$ viewed along [100] (on top). The Er^{3+} ions are connected to layers by tridentate (light grey tetrahedra) and bidentate (dark grey tetrahedra) selenate ions. The layers $Er_2(SeO_4)_3 \cdot 8H_2O$ are stacked in the [201] direction and linked only *via* hydrogen bonds (at bottom).

lenate ions, $Se(2)O_4^{2-}$, is located on a special position (4*e*) of the space group $C2/c$, the second one, $Se(1)O_4^{2-}$, resides on a general site (8*f*) (Table 2). The $Se(1)O_4^{2-}$ anion connects three Er^{3+} ions with each other, $Se(2)O_4^{2-}$ only two, leading to layers according to $^2_\infty[Er(H_2O)_{4/1}(Se(1)O_4)_{3/3}(Se(2)O_4)_{1/2}]$ (Fig. 1). Within the selenate ions typical distances Se-O between 161.9(7) and 166.6(7) pm are observed (Table 3). The angles O-Se-O show also the expected values (106.5(4)° to 113.1(6)°) and prove that the tetrahedra are only slightly distorted. The layers are connected *via* hydrogen bonds, and even if the hydrogen

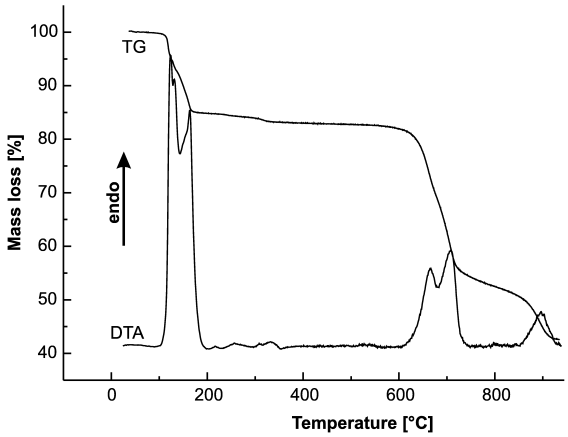

Fig. 2. DTA/TG diagram for the thermal decomposition of $Er_2(SeO_4)_3 \cdot 8H_2O$. The two steps between 100 and 200 °C indicate dehydration of the compound. The degradation of $Er_2(SeO_4)_3$ leads to the oxide Er_2O_3 with $Er_2(SeO_3)_3$ and $Er_2(SeO_3)O_2$ as intermediates (see also Table 4).

atoms of the H_2O molecules could not be located, it can be assumed that the non-coordinating oxygen atoms of the selenate ions act as acceptors and the water molecules as donors, in accordance with the findings for $Er_2(SO_4)_3 \cdot 8H_2O$ [12].

Thermal behaviour

According to the DTA/TG measurement the thermal decomposition of $Er_2(SeO_4)_3 \cdot 8H_2O$ starts at 122 °C with the loss of the crystal water (Fig. 2, Table 4). The dehydration is a two–step process, although a little shoulder is discernible in the DTA curve for the first step. With respect to the mass loss the intermediate is the trihydrate, $Er_2(SeO_4)_3 \cdot 3H_2O$. A two−step dehydration has been observed also for $Er_2(SO_4)_3 \cdot 8H_2O$, but in contrast to the latter the onset temperature for the dehydration is about 20 °C higher in the present case and the resolution of the two steps in both DTA and TG curve is not clearly observable. This is also reflected by the temperature dependent X-ray powder diffraction experiment which does not allow the detection of the diffractogram of $Er_2(SeO_4)_3 \cdot 3H_2O$, although this was possible for the sulfate trihydrate.

The dehydration is complete at 213 °C and leads to the anhydrous selenate $Er_2(SeO_4)_3$. In the powder diffraction investigation the pattern of $Er_2(SeO_4)_3$ can be detected at 175 °C and the diffractogram can be indexed unambiguously assuming the trigonal-rhombohedral structure of $Sc_2(SO_4)_3$ [13]. The latter

Reaction	T_{onset} [°C]	T_{end} [°C]	T_{max} [°C]	Mass loss/% obsd.	calcd.
$Er_2(SeO_4)_3 \cdot 8H_2O \xrightarrow[-5H_2O]{} Er_2(SeO_4)_3 \cdot 3H_2O$	122	172	157	10.0	9.9
$Er_2(SeO_4)_3 \cdot 3H_2O \xrightarrow[-3H_2O]{} Er_2(SeO_4)_3$	157	213	192	15.6	15.9
$Er_2(SeO_4)_3 \xrightarrow[-3/2O_2]{} Er_2(SeO_3)_3$	658	681	686	23.8	21.2
$Er_2(SeO_3)_3 \xrightarrow[-2SeO_2]{} Er_2(SeO_3)O_2$	682	777	737	54.8	54.4
$Er_2(SeO_3)O_2 \xrightarrow[-SeO_2]{} Er_2O_3$	916	959	947	56.6	57.8

Table 4. DTA/TG results of the thermal decomposition of $Er_2(SeO_4)_3 \cdot 8H_2O$.

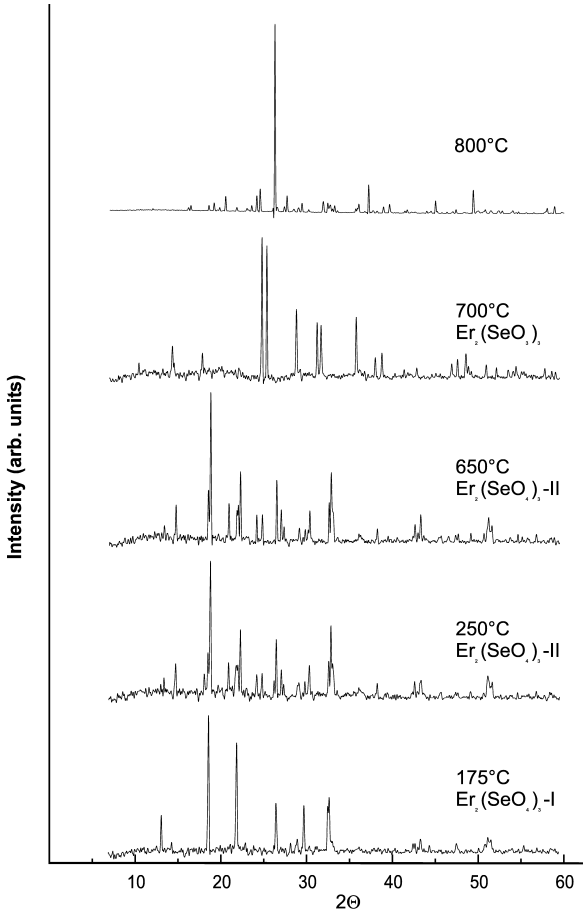

Fig. 3. Temperature dependent X-ray diffraction diagrams monitoring the decomposition of $Er_2(SeO_4)_3 \cdot 8H_2O$. At 175 °C the diffractogram of the trigonal-rhombohedral modification of $Er_2(SeO_4)_3$ is observed. $Er_2(SeO_4)_3$ undergoes a phase transition to an orthorhombic modification which exists up to 650 °C. At 700 °C the diffractogram of $Er_2(SeO_3)_3$ occurs and at 800 °C a new compound has formed, probably the structurally unknown oxide-selenite $Er_2(SeO_3)O_2$. (see also Table 5).

is different from the one determined from single crystal data of $Er_2(SO_4)_3$ which is orthorhombic. Interestingly it has also been observed for $Er_2(SO_4)_3 \cdot 8H_2O$ that the dehydration leads to $Er_2(SO_4)_3$ in the trigonal-rhomohedral form (I) proving the dimorphism of the sulfate. The same dimorphism occurs for $Er_2(SeO_4)_3$ as may be seen from the diffractogram at 250 °C (Fig. 3). This pattern shows clearly the orthorhombic modification of $Er_2(SeO_4)_3$ (II). The structures of the two modifications of $Er_2(SeO_4)_3$ are very similar as it has been described in more detail for the pair $Sc_2(SO_4)_3/Y_2(SO_4)_3$ [13]. The coordination is octahedral in both cases and the kind of linkage of $[ErO_6]$ octahedra and $[SeO_4]$ tetrahedra remains the same. That might be the reason why the phase transition cannot be observed in the DTA curve. A further noteworthy detail of the temperature dependent X-ray diffraction can be seen from the refined lattice parameters: The values for $Er_2(SeO_4)_3$-I decrease when going from 175 to 200 °C, indicating negative thermal expansion. The same effect has been observed for $Er_2(SO_4)_3$-I [12] and in more detail for $Sc_2(SO_4)_3$ [14]. On the other hand, $Er_2(SeO_4)_3$-II exhibits a volume expansion with increasing temperature that interestingly is due to the lengthening of only the *a*–axis while the other two axes remain the same within the standard deviations.

The orthorhombic form of $Er_2(SeO_4)_3$ exists up to 658 °C when the decomposition to $Er_2(SeO_3)_3$ is observed in the DTA/TG measurements (Table 4). However, the respective effect is severely obscured by that of a second step that indicates the formation of the oxide–selenite $Er_2(SeO_3)O_2$ between 682 and 777 °C (Fig. 2). Nevertheless, the powder diffractograms at 700 and even at 750 °C can be unambiguously assigned to $Er_2(SeO_3)_3$ whose crystal structure has recently been reported [4]. The difference in the results of the DTA and powder diffraction measurements may be attributed to the different conditions of the two methods. The diffractogram at 800 °C shows a new phase, which probably is $Er_2(SeO_3)O_2$ as suggested by the DTA data. Above 900 °C, Er_2O_3 is found as the final product of the thermal decomposition.

Table 5. Refined lattice parameters of the thermal decomposition products of $Er_2(SeO_4)_3 \cdot 8H_2O$ (X-ray powder data).

T [°C]	Compound	Space group	a [pm]	b [pm]	c [pm]	α [°]	β [°]	γ [°]
50	$Er_2(SeO_4)_3 \cdot 8H_2O$	$C2/c$	1373.2(5)	687.1(2)	1861.2(4)		101.84(3)	
75	$Er_2(SeO_4)_3 \cdot 8H_2O$	$C2/c$	1375.6(6)	688.5(2)	1863.2(5)		101.82(3)	
100	$Er_2(SeO_4)_3 \cdot 8H_2O$	$C2/c$	1377.9(6)	689.1(3)	1864.2(5)		101.81(3)	
125	$Er_2(SeO_4)_3 \cdot 8H_2O$	$C2/c$	1378.8(7)	689.8(4)	1866.3(6)		101.85(4)	
150	$Er_2(SeO_4)_3 \cdot 8H_2O$	$C2/c$	1380.1(7)	691.3(4)	1868.3(7)		101.83(4)	
175	$Er_2(SeO_4)_3$-I	$R\bar{3}$	939.9(3)		2427.1(4)			
200	$Er_2(SeO_4)_3$-I	$R\bar{3}$	938.2(3)		2424.6(5)			
250	$Er_2(SeO_4)_3$-II	$Pbcn$	1313.5(3)	955.2(3)	943.2(3)			
300	$Er_2(SeO_4)_3$-II	$Pbcn$	1315.4(4)	955.8(4)	944.9(3)			
350	$Er_2(SeO_4)_3$-II	$Pbcn$	1316.2(4)	955.4(3)	944.6(3)			
400	$Er_2(SeO_4)_3$-II	$Pbcn$	1316.6(4)	955.5(3)	944.7(3)			
450	$Er_2(SeO_4)_3$-II	$Pbcn$	1316.9(4)	954.6(3)	945.0(4)			
500	$Er_2(SeO_4)_3$-II	$Pbcn$	1317.7(4)	954.6(3)	944.9(4)			
550	$Er_2(SeO_4)_3$-II	$Pbcn$	1318.0(5)	954.8(4)	944.9(3)			
600	$Er_2(SeO_4)_3$-II	$Pbcn$	1318.4(4)	954.7(4)	944.8(3)			
650	$Er_2(SeO_4)_3$-II	$Pb\underline{c}n$	1318.9(4)	954.8(5)	944.9(4)			
700	$Er_2(SeO_3)_3$	$P\bar{1}$	701.6(2)	814.4(2)	937.8(2)	69.82(2)	67.51(2)	64.40(3)
750	$Er_2(SeO_3)_3$	$P1$	703.2(3)	815.5(2)	939.1(3)	69.93(2)	67.47(2)	64.80(4)

Our current investigations aim at the preparation of $Er_2(SeO_4)_3$ and $Er_2(SeO_3)O_2$ in single crystalline form in order to allow a complete characterization of the observed intermediates.

Acknowledgments

The authors are indebted to Prof. Dr. G. Meyer and the Fonds der Chemischen Industrie, Frankfurt am Main, for generous support. Furthermore, this work has been supported by the Deutsche Forschungsgemeinschaft (Graduiertenkolleg 549). The technical assistance of Mrs. I. Müller is also gratefully acknowledged.

[1] M. S. Wickleder, Chem. Rev. **102**, 2011 (2002), and references therein.

[2] W. W. Wendtlandt, J. Inorg. Nucl. Chem. **7**, 51 (1958); H. G. Brittain, J. Less-Common Met. **93**, 97 (1983); L. Niinistö, P. Saikkonen, P. Sonninen, Proc. Acad. Sci. Est. SSR Chem. **33**, 209 (1984); N. Bukovec, P. Bukovec, J. Siftar, Vestn. Slov. Kem. Drus. **22**, 5 (1975); L. Niinistö, P. Saikkonen, P. Sonninen, Rare Earths Mod. Sci. Techn. **3**, 257 (1982). H.-U. Hummel, E. Fischer, T. Fischer, P. Joerg, G. Pezzei, Z. Anorg. Allg. Chem. **619**, 805 (1993).

[3] I. Giolito, E. Giesbrecht, An. Acad. Brasil. Ciênc. **41**, 517 (1969); M. A. Nabar, S. V. Paralkar, Thermochim. Acta **15**, 390 (1976); M. A. Nabar, S. V. Paralkar, Thermochim. Acta **15**, 239 (1976); L. Niinistö, P. Saikkonen, R. Sonninen, Rare Earths Mod. Sci. Techn. **3**, 257 (1982); S. Karvinen, L. Niinistö, Lanth. Actin. Res. **1**, 169 (1986).

[4] M. S. Wickleder, Z. Anorg. Allg. Chem. **626**, 547 (2000); I. Krügermann, M. S. Wickleder, J. Solid State Chem. **167**, 113 (2002).

[5] H. Oppermann, M. Zhang-Preße, S. Weck, S. Liebig, Z. Anorg. Allg. Chem. **628**, 81 (2001); H. Oppermann, M. Zhang-Preße, Z. Naturforsch. **56b**, 917 (2001); M. Zhang-Preße, H. Oppermann, J. Therm. Anal. Cal. **69**, 301 (2002); H. Oppermann, M. Zhang-Preße, Z. Naturforsch. **57b**, 661 (2002).

[6] J. Wontcheu, Th. Schleid, Z. Anorg. Allg. Chem. **628**, 1941 (2002).

[7] G. Bauer (ed.), Handbuch der Praparativen Anorganischen Chemie, Bd. I, F. Enke Verlag, Stuttgart (1975).

[8] G. M. Sheldrick, SHELXS86, Programs for X-ray structure analysis, Göttingen (1986); G. M. Sheldrick, SHELXL93, Program for the Refinement of Crystal Structures, Göttingen (1993).

[9] X-RED 1.07, Data Reduction for STADI4 and IPDS, Stoe & Cie, Darmstadt (1996); X-SHAPE 1.01, Crystal Optimisation for Numerical Absorption Correction, Stoe & Cie, Darmstadt (1996).

[10] Thermal analysis for the analyzer STA 409, version 3.1, NETZSCH GmbH, Selb, Germany (1996).

[11] VISUAL X^{POW} 3.01, software package for the STOE powder diffraction system, Stoe & Cie, Darmstadt, Germany (1996).

[12] M. S. Wickleder, Z. Anorg. Allg. Chem. **625**, 1548 (1999).

[13] M. S. Wickleder, Z. Anorg. Allg. Chem. **626**, 1468 (2000).

[14] M. S. Wickleder, U. Ruschewitz, unpublished results.

[15] Th. Hahn (ed.), International Tables for Crystallography, Vol. C, D. Reidel Publishing Company, Dordrecht, Boston (1983).

[16] R. X. Fischer, E. Tillmanns, Acta Crystallogr. **C44**, 775 (1988).